



Article citation info:

Karabacak Y. E, Deep learning-based CNC milling tool wear stage estimation with multi-signal analysis, *Eksploracja i Niezawodność – Maintenance and Reliability* 2023; 25(3) <http://doi.org/10.17531/ein/168082>

Deep learning-based CNC milling tool wear stage estimation with multi-signal analysis

Indexed by:



Yunus Emre Karabacak^{a,*}

^aDepartment of Mechanical Engineering, Karadeniz Technical University, Turkey

Highlights

- The convolutional neural network (CNN) was performed to detect the wear stages of the milling tool.
- Short Time Fourier Transform (STFT) was applied to signals, and signal spectrograms were used to train CNN models.
- Pre-trained CNNs (GoogleNet, AlexNet, ResNet-50, and EfficientNet-B0) detected the tool wear stage with varying accuracies.
- CNN shows promise for condition monitoring of milling operations and detecting tool wear stage.

Abstract

CNC milling machines are frequently used in the manufacturing of mechanical parts in the industry. One of the most important components of milling machines is the cutting tool. Monitoring the cutting tool wear is important for the reliability, continuity, and quality of production. Monitoring the tool and detecting the stage of wear are difficult processes. In this work, the convolutional neural network (CNN), which is a deep learning method in which the features are extracted by an inner process, was performed to detect the wear stages of the milling tool. These stages that define the total lifespan of the tool are known as initial wear (IW), steady-state wear (SSW), and accelerated wear (AW). Short Time Fourier Transform (STFT) was applied to signals, and signal spectrograms were used to train CNN models with different complex architectures. Vibration signals, acoustic emission signals, and motor current signals from The Nasa Ames Milling Dataset were used to obtain the spectrograms. Pre-trained CNNs (GoogleNet, AlexNet, ResNet-50, and EfficientNet-B0) detected the tool wear stage with varying accuracies. It has been seen that the time duration of model training increases as the size of the dataset grows and the network architecture becomes more complex. The recommended method has also been tested on the 2010 PHM Data Challenge Dataset. CNN shows promise for condition monitoring of milling operations and detecting tool wear stage.

Keywords

wear stage estimation, milling, convolutional neural network, time-frequency analysis

This is an open access article under the CC BY license (<https://creativecommons.org/licenses/by/4.0/>)

1. Introduction

Industrial condition monitoring systems are developing in parallel with advancing technology and artificial intelligence applications. The effective use of condition monitoring and machine learning systems is increasing in machines or production facilities where continuous, uninterrupted, and error-free operation is desired [6]. Monitoring milling tool wear has become day-by-day important in smart manufacturing systems to enhance product reliability and efficiency. During

the machining process, damaged or worn tools can result in a poor surface finish on the workpiece and even product wastage. Therefore, tool wear is monitored in real-time in smart manufacturing. To prevent the negative impact of tool damage on the machining process, online monitoring systems can be used [46].

The tool condition changes depending on factors such as the speed of cutting, cutting depth, the material of the workpiece,

(*) Corresponding author.

E-mail addresses:

Y. Emre Karabacak (ORCID:0000-0002-0268-3656) karabacak@ktu.edu.tr

and the geometrical properties of the tool. Taking these parameters into account, the tool wear stage can be diagnosed in real-time using measurements such as cutting force, vibration signal, acoustic emission signal, and spindle motor current signal [45]. Vision-based techniques such as the contactless optical method, laser scattering pattern, scanning electron microscopy, and optoelectronic imaging are also used in the investigation and analysis of more complex and unpredictable tool faults [44]. Sensors used for measurements such as accelerometers, ultrasonic sensors, and current sensors are critical components of data acquisition and tool condition monitoring systems. Time, frequency, and time-frequency domain features are obtained from the signals acquired from these sensors, and these features are utilized in the analysis, classification, and estimation of the tool wear [41]. With different approaches in time or frequency domain analysis of signals, features can be extracted manually or automatically from experimental data and used in different decision-making algorithms to estimate tool conditions [16]. Determining the decision-making algorithm is one of the essential phases in the condition monitoring of the tool. Algorithms such as Artificial Neural Networks (ANNs) [7], Long Short-Term Memory Networks (LSTMs) [63], Support Vector Machines (SVMs) [37,65], Gaussian Process Regression (GPR) [34], Decision Trees [33], Fuzzy Logic [3,13], Genetic Algorithm (GA) [53], Hidden Markov Model (HMM) [36], and Adaptive Network Based Fuzzy Inference Systems (ANFIS) [56] have been used to estimate tool wear.

There are also deep learning-based methods in which features are automatically extracted from signals or images, such as Recurrent Neural Networks (RNNs), Deep Multi-layer Perceptron, Deep Reinforcement Learning, and Convolutional Neural Networks (CNNs) [48]. In recent years, the amount of studies on the application of CNN in tool wear estimation has increased [55]. Liu et al. [39] conducted a new CNN-transformer neural network model to obtain a more suitable tool wear estimation. In this model, they used the transformer model and convolutional neural networks together to obtain condition monitoring data such as shear force in parallel. Yin et al. [60] performed multi-sensor-based tool wear detection using one-dimensional CNN and deep generalized canonical correlation analysis. Experiments showed that their performed approach

can acquire sufficient accuracy and real-time implementation. Terrazas et al. [51] presented an online tool wear estimation method by using condition monitoring for dry milling of steel. In their study, they preferred the CNN approach to determine flank wear by using cutting force measurements. Cao et al. [12] conducted a new intelligent system for tool wear condition monitoring by utilizing spindle vibration signals. In this system, they combined wavelet frames with CNN. They utilized CNN to apply a deep learning approach to 2D vibration images and observed that with the integration of wavelet frames and CNN, tool wear stages can be effectively diagnosed. Wu et al. [57] conducted a CNN tool wear estimation model by using an image dataset and utilized a convolutional autoencoder to pre-train the network model. They also used the backpropagation algorithm integrated with the stochastic gradient descent algorithm to fine-tune the model parameters. Experimental findings demonstrated that the average identification performance of the model is sufficient, and the model had the ability to recognition of tool wear types. Brili et al. [10] performed automatic identification of tool wear based on infrared thermography and CNN, while the turning operation. The CNN model automatically determines the wear stage of the turning tool by using thermographic image data. The accuracy of the classification confirmed the adequacy of the proposed method. Aghazadeh et al. [2] investigated a powerful milling tool wear estimation method by using CNNs. They proposed a mixed feature extraction approach based on wavelet time-frequency transform and spectral extraction algorithms to concentrate the influence of tool wear in the signal and decrease the influence of other milling factors. They finally validated their research using different datasets. Huang et al. [27] conducted a tool wear estimation system in milling operations by using short-time Fourier transform (STFT) and CNN by using vibration signals. First, image representations of vibration signals were obtained by using STFT. These images were then utilized for feature extraction to estimate tool wear automatically by using CNN. Dai et al. [18] performed a CNN-based monitoring method to recognize intermediate anomalies and estimate tool wear in aerospace-related multi-stage manufacturing processes. Using their proposed approach, they expanded the criteria for evaluating anomalous conditions for practical applications and increased recognition stability through features. Cao et al. [11]

introduced a powerful milling tool wear estimation system by using two-dimensional CNN and derived wavelet frames. With their proposed methodology, they achieved sufficient recognition accuracy and confirmed that the derived wavelet frames were effective. Duan et al. [19] conducted a new deep-learning approach by using the multi-frequency band technique and CNN to process signal data and estimate tool wear. In this model, signal samples are augmented and wavelet packet decomposition is used to get wavelet coefficients in varied frequency bands, and CNN is used for precise feature extraction from these coefficients. In their study, Bazi et al. [8] proposed a new method with CNN and bidirectional long short-term memory applications to estimate tool wear while cutting operations. To avoid the obstacles of time-consuming manual feature fusion, Li et al. [35] conducted a new tool wear monitoring approach by using multi-domain feature fusion with depth-wise separable CNN. With this method, they obtained frequency and time domain features from shear force and vibration signals and combined feature tensors. Lim et al. [38] enhanced the deep learning regression approach to estimate tool wear through features obtained from 2D visual data of the workpiece's surface. They compared the models developed based on CNN and deep neural networks for predictive accuracy. Ambadekar and Choudhari [5] proposed an estimation method to estimate the flank wear of the cutting tool with CNN. They used carbide inserts as cutting tools in their work and carried out the experiments under dry conditions. To detect the development of flank wear, visual data of the cutting tool and workpiece were acquired at constant intervals by utilizing a microscope. Images collected in one of three wear classes, low, medium, and high, were used as inputs to the CNN tool monitoring model. Bergs et al. [9] investigated a deep learning method for 2D visual data processing to determine tool wear conditions. Accordingly, they trained a CNN to classify the cutting tool wear stages. As a result of the evaluation they made with the test dataset, they reached a satisfactory result. Huang et al. [28] conducted a new tool wear estimation approach by using multi-domain feature fusion with CNN. They showed that with this method, the low prediction accuracy seen in manual feature fusion can be avoided and the tool state can be predicted effectively. Huang et al. [29] used reshaped time series signals in another study and presented a multisensory tool wear

estimation approach by using CNN. Xu et al. [58] improved a tool wear estimation system by using a deep learning method for industrial applications. They performed multiscale feature fusion with CNN and improved the prediction results. Cooper et al. [17] conducted a CNN-based tool wear estimation model for vertical machining workings by utilizing acoustic emission signals. Ma et al. [40] conducted the mechanism of tool wear in the milling operations of a titanium alloy. They developed two new tool wear estimation models by using deep learning utilizing a convolutional bidirectional long short-term memory network and a convolutional bidirectional gated recurrent unit. Huang and Lee [26] presented a study in which they estimated the tool wear formation and roughness of the surface by using vibration signals and sound signals with deep learning and sensor fusion approaches. The realized design was used for online condition monitoring of the tool via an alarm. Zhou et al. [64] conducted a tool wear estimation system by using deep learning and limited samples of cutting force time series signals. The multi-scale edge labeling graph neural network achieved more satisfactory accuracy results than CNN-based methods with a small number of time series signals.

In tool wear estimation and remaining useful life studies, various selection techniques are required to determine ideal features. In the case of using classical algorithms, the features are calculated and selected manually. In this case, negativities such as computational complexity and errors cause low model accuracy and time loss. Deep learning methods such as CNN eliminate remove disadvantages and achieve successful results even when limited data are used [4]. Deep learning mostly needs big data and training time is longer than conventional machine learning algorithms. However, it is thought that these disadvantages will be overcome with the development of high-performance computers in the future [59,62].

Understanding the variation of signals in time and time-frequency domain is very important in monitoring tool condition and detecting wear stage. Because the changes in the signals with the wear of the tool manifest themselves in the time and time-frequency domain. The model is successful if the signals are evaluated effectively and the features are obtained error-free and fast. For this reason, the deep learning method based on convolutional neural networks, in which features are automatically extracted from 2D visual data, will allow us to

obtain more successful results than other studies in the literature. The wear data collected in the machining process is in a non-linear and time-varying form. For this reason, the wear process of the tool should be evaluated as stages and the signal features of each stage should be classified accordingly. There is no study in the literature that considers different wear stages holistically. Whether the tool wear pattern is ultimately suitable depends not only on accurate results but also on being fast and practical. In industrial plants with time pressure and working in shifts, tool wear needs to be determined accurately and at the right time. There has not been a study in the literature in which learning models were evaluated comparatively in this respect.

In this study, different CNN models were trained for tool wear stage estimation using vibration data, acoustic emission data, and motor current data in The Nasa Ames Milling Dataset [21]. In the proposed method, STFT was applied to all signal data and 2D spectrograms were obtained. The tool wear stages are designated as the initial wear stage (IW), steady state wear stage (SSW), and accelerated wear stage (AW). Unlike the literature, CNN models with different architectures (GoogleNet, ResNet-50, AlexNet, and EfficientNet-B0) were trained with spectrograms, used for tool wear stage estimation, and comparatively examined in terms of complexity, training time, testing, and verification performance. Different CNN models were also trained for tool wear stage estimation using cutting force data, vibration data, and acoustic emission data from the 2010 PHM Data Challenge Dataset.

2. Method and Material

2.1 Tool Wear Mechanism

During milling, the forces and temperature caused by the surface deformation and friction between the tool and the workpiece directly affect the milling tool's life [24,43]. The milling tool is also affected by chemical reactions occurring on the contact surfaces. As a result, tool wear gradually develops due to mechanical (adhesion, abrasion, fatigue, plastic deformation, etc.) thermal (thermo-mechanical), and chemical (diffusion, oxidation, etc.) factors [47,50].

In machining operations with a worn tool, cutting forces increase, the surface quality of the workpiece decreases and it becomes difficult to manufacture within tolerances. Consequently, it is required to detect cutting tool wear on time and replace it. Wear types such as flank wear, crater wear, groove wear, notch wear, and nose wear can take place on the cutting tool. The stage of flank wear (VB) is an important indicator for monitoring tool condition and is the best parameter for replacement decisions [52].

The change of tool wear over time can be considered a continuous function or it can be evaluated as stages. For this reason, in many searches in the literature, tool flank wear is evaluated in stages as initial wear (IW), steady state wear (SSW), and accelerated wear (AW) [14,42]. The development of these stages of the milling tool is not an accidental process. Fig. 1 shows the milling operation (a) and tool wear stages (b). Accordingly, the first region is the IW stage where wear appears. The second region is the SSW stage, in which wear progresses at a uniform rate. The third region, in which wear takes place at a gradually growing rate, is the AW stage [49].

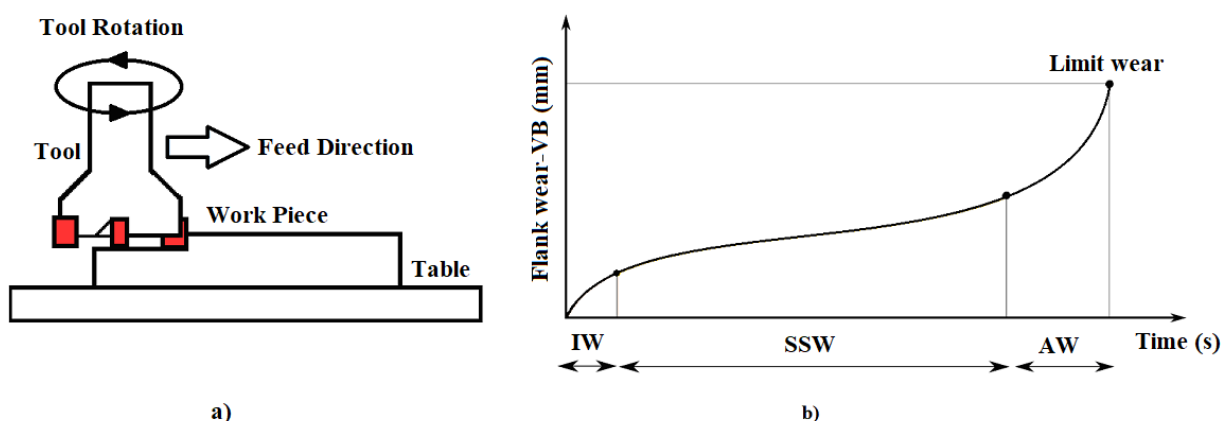


Fig. 1. The milling operation (a) and tool wear stages (b) [16].

2.2 The NASA Ames Milling Dataset and Experimental System

The Nasa Ames Milling Dataset was used to validate the proposed methods in this study. The Nasa Ames Milling Dataset was obtained from experimental studies performed under different operating conditions. In the experiments, tool wear was evaluated with a microscope regularly after any cutting operation. Different sensors, namely acoustic emission sensors, vibration sensors, and spindle motor current sensors, were placed at various locations of the milling machine and used for measurements. The collected data were arranged as a Matlab struct array and made available for analysis. The experimental studies were conducted in a total of 16 cases (166 runs) and the flank wear (VB) was measured after the runs in each case. The experimental duration was set as 1 s for each run and restarted for each experiment [21]. Details on feed, depth of cut, workpiece materials, and measurement sensors in the experimental studies are presented in Table 1.

Table 1 Details of the experimental system [21].

Case	Run	Cut Depth (mm)	Feed (mm/rev)	Materials	Acoustic Emission Sensors	Vibration Sensors	Motor Current Sensors
1 to 16	166	0.75-1.5	0.25-0.5	Steel and cast iron	Spindle and table	Spindle and table	AC and DC

The details of the data acquisition system are given in Fig. 2.

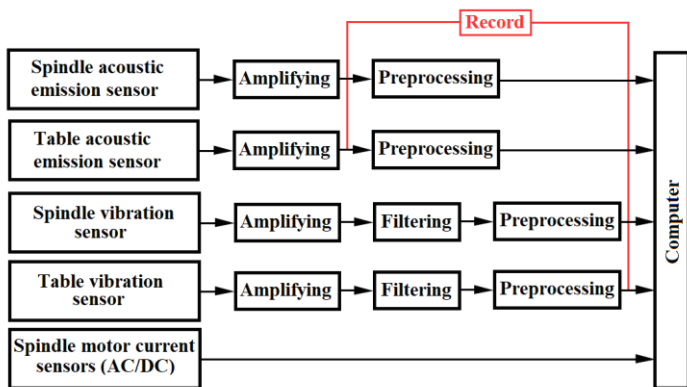


Fig. 2. Details of data acquisition system [21].

The signals from vibration sensors are amplified, filtered, and preprocessed before entering the computer. The signals from acoustic emission sensors are amplified and preprocessed before entering the computer for data acquisition. The signals from the spindle motor current sensors are sent to the computer without being processed [21]. More information about the other constituents of the experimental setup and the data set can be found in the cited reference.

2.3 The 2010 PHM Data Challenge Dataset and Experimental System

The 2010 PHM Data Challenge is another dataset used to validate the methods proposed in this study [1]. The 2010 PHM Data Challenge Dataset is derived from experimental studies performed under consistent operating conditions. The details of the experimental system can be seen in Fig. 3. A three-flute ball nose tungsten carbide milling cutter was used in the experiments. The working parameters were set as given in Table 2.

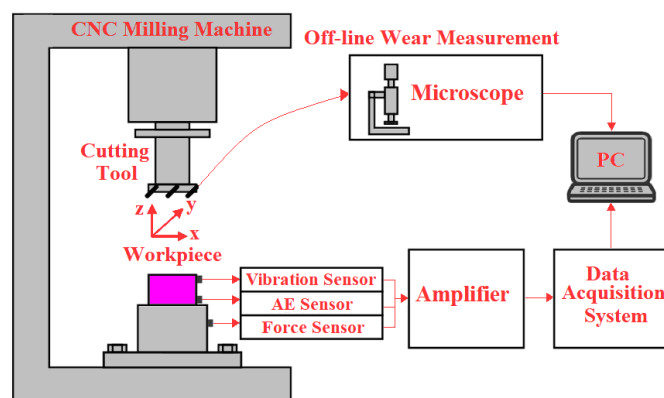


Fig. 3 Details of The 2010 PHM Data Challenge experimental system [54].

Table 2 Details of the experimental system [1,54].

The Spindle Running Speed [rpm]	The Rate of Feed [mm/min]	The Depth of Cut (Radial) (mm)	The Depth of Cut (Axial) (mm)
10400	1555 (x-direction)	0.125 (y-direction)	0.2 (z-direction)

Cutting forces are measured in the x, y and z axes with a 3-component platform dynamometer placed between the workpiece and the machining table. Machine tool vibrations during the cutting process are measured with three accelerometers mounted on the workpiece in the x, y, and z directions. An acoustic emission sensor is also attached to the workpiece to monitor the acoustic emission produced by the cutting process. Vibration, force, and acoustic emission signals are transmitted to the PC after preprocessing in a charge amplifier and data acquisition system. The sampling rate of the data acquisition system is 96 kHz. The flank wear of each flute was measured after the finishing of machining each surface. Signals were acquired using 7 channels, and flank wear was assigned as the target value of these signals [1,54].

2.4 Time-Frequency Signal Analysis

In this study, time-frequency domain analysis of different

source signals acquired from the milling experiment system for tool wear stage estimation was performed. So, Short Time Fourier Transform (STFT) was applied to vibration, acoustic emission, and motor current signals, and 2D spectrograms were obtained for different operating conditions. After the spectrograms of each signal type were recorded as 2D data, they were used as a dataset for training the CNN models. STFT is performed by dividing the signal into short segments and applying the Fourier transform for each segment [30]. Fig. 4 shows the STFT of a time domain signal.

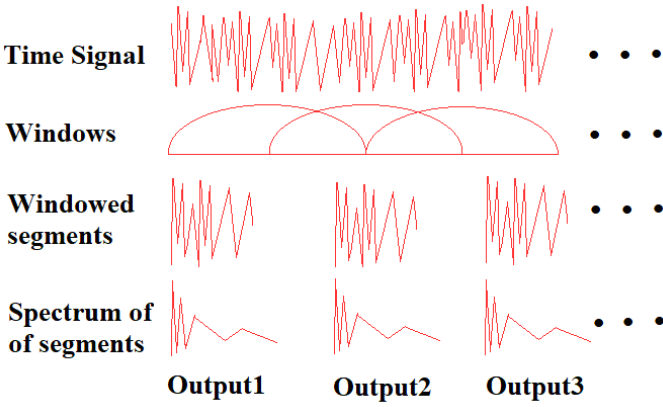


Fig. 4. Example of STFT of a time domain signal.

For the continuous-time case, the STFT is obtained by multiplication the signal with a window function. In Eq. (1), $x(t)$ indicates the time domain signal, ω represents frequency, τ indicates the time index, and $W(t)$ represents the window function [32].

$$STFT\{x(t)\}(\tau, \omega) = \int_{-\infty}^{+\infty} x(t)W(t - \tau)e^{-j\omega t} dt \quad (1)$$

In the case of discrete time, STFT can be calculated as in Eq. (2). Here, the discrete signal is represented by $x[k]$, and the window function is represented by $W(k)$. The discrete-time intervals are represented by k , and l . Accordingly, the 2D spectrogram of the STFT function can be obtained by using Eq. (3) [32].

$$STFT\{x[t]\}(l, \omega) = X(l, \omega) = \sum_{-\infty}^{+\infty} x[k]W(k - l)e^{-j\omega k} \quad (2)$$

$$Spectrogram\{x[t]\}(l, \omega) = |X(l, \omega)|^2 \quad (3)$$

2.5 Convolutional Neural Networks (CNNs)

Convolutional neural networks (CNNs) are a special subclass of the deep learning approach and are usually utilized for classification or regression analysis on images. CNN, one of the most used types of machine learning, was created by developing

multi-layer perceptrons in a certain order. In multilayer perceptrons, every neuron in a particular layer is bonded to all neurons in the following layer. CNN comprises convolutional and subsampling layers. Convolutional and subsampling layers have a specific topographic system, and each layer contains different clusters of neurons. Every neuron is also bonded to neurons in prior layers. Fig. 5 indicates an ordinary CNN architecture including an input layer, convolution layer, pooling layer, fully connected layer, and output layer. In the case of using the CNN algorithm, there is no need to manually calculate the features for tool wear stage estimation. Depending on the features that CNN chooses within itself, better results can be obtained, it can reduce the computational complexity and prevent overfitting with validation [20,23].

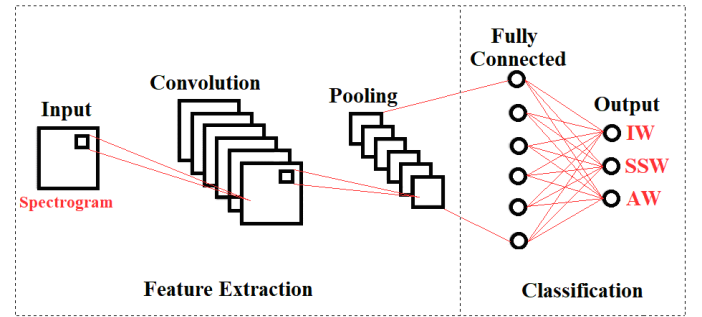


Fig. 5. Typical CNN architecture.

Convolutional layers comprise a series of filters. These filters multiply the inputs from the prior layer by weights and create an output entitled feature map. The filter neurons are connected to the input data and the values of these data are multiplied by weights. Since every neuron in the same filter shares its weights, the optimization time is shortened and the complexity of CNN is decreased [59].

If the input to the convolution layer is considered to be $X \in R^{A \times B}$, the layer output is calculated as in Eq. (4). Here, A and B demonstrate the input data dimensions, $*$ represents the convolution operator, C_n represents the n th feature map of the convolution layer, X represents the input data matrix, w_n represents the weight matrix of the n th filter of the actual layer, b_n represents the n th bias, and f demonstrates the nonlinear activation function implemented to the result [31].

$$C_n = f(X * w_n + b_n) \quad (4)$$

The pooling layers follow the convolution layers and decrease the dimensions of the network features and network parameters by subsampling. The maximum pooling is the most

preferred function in CNN for calculating activation statistics. The maximum pooling activation function can be given as in Eq. (5). Here, S demonstrates the pooling block dimension, and $C_n \in S$, P_n represents the pooling layer output [31].

$$P_n = \max C_n \quad (5)$$

The fully connected layer comes after the convolution and pooling layers. This layer can be collated with traditional neural networks. Therefore, it can be implemented for problems dealing with classification and regression. In this study, one hidden layer and softmax regression were utilized as the final layer. Since the milling tool wear stage is classified, the softmax regression output can be written as in Eq. (6). Here, H represents the number of the wear stage class label, w_j represents the weight matrix, b_j represents the bias, and R demonstrates the

result of the classification the tool wear stage [31].

$$R = \begin{bmatrix} P(y = 1|x; w_1, b_1) \\ P(y = 2|x; w_2, b_2) \\ \dots \\ P(y = H|x; w_H, b_H) \end{bmatrix} \frac{1}{\sum_{j=1}^H \exp(w_j x + b_j)} \begin{bmatrix} \exp(w_1 x + b_1) \\ \exp(w_2 x + b_2) \\ \dots \\ \exp(w_H x + b_H) \end{bmatrix} \quad (6)$$

2.6 Tool Wear Stage Estimation with Modified Pre-trained CNNs

Pre-trained CNN models can be modified and used for new regression and classification problems. Thus, the time and effort required to develop and train an entirely new network become less [25]. Therefore, in this study, pre-trained CNNs were used for tool wear stage classification. The specifications for these CNNs are given in Fig. 6 and Table 3.

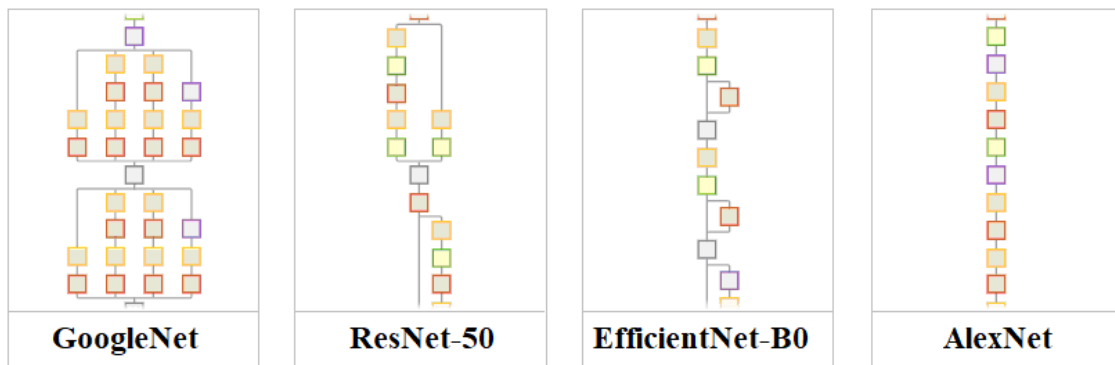


Fig. 6. Pre-trained CNNs.

Table 3. Modified CNN specifications.

	GoogleNet	ResNet-50	AlexNet	EfficientNet-B0
Layer depth	22	50	8	82
Layer number	144	177	25	290
Connection number	170	192	24	362
Type of input	2D Spectrogram	2D Spectrogram	2D Spectrogram	2D Spectrogram
Size of input	224x224x3	224x224x3	227x227x3	224x224x3
Type of output	Classification	Classification	Classification	Classification
Size of output	3 (Wear Stages)	3 (Wear Stages)	3 (Wear Stages)	3 (Wear Stages)
The factor of weight learning rate	10	10	10	10
The factor of bias learning rate	10	10	10	10
Loss function	Cross Entropy	Cross Entropy	Cross Entropy	Cross Entropy

The amount of data used in training CNNs is usually quite large. However, it is also possible to train CNNs with a relatively limited number of 2D data. In the case of using a limited number of 2D data, CNN training performance can be

increased by fine-tuning the hyperparameters of the network and increasing the resolution of the 2D data [30,59]. To enhance the performance of the pre-trained CNNs utilized in this study,

firstly, the network hyperparameters were updated with fine-tuning, and data augmentation was applied to the 2D spectrograms. Details on the training parameters of pre-trained CNNs can be seen in Table 4. In addition, 50% of the

spectrograms of the signals were used for training the networks. 30% of the remaining spectrograms were used for validation, and 20% for testing.

	GoogleNet	ResNet-50	AlexNet	EfficientNet-B0
Frequency of Validation	5 Hz			
Rate of Learning	0.001			
Maximum Epoch	5			
Size of Mini Batch	10			
Input Data Resolution	489 x 435 pixel (2D Spectrogram)			

Table 5 indicates the output and input details of the CNN models for The Nasa Ames Milling Dataset. Spectrograms of vibration signals, acoustic emission signals, and motor current signals were obtained separately as 2D visual data. They are split into three parts as training, validation, and testing. CNN outputs were modified to classify the tool wear stage.

Accordingly, wear values between 0 mm and 0.19 mm in The Nasa Ames Milling Dataset were considered IW. Wear values between 0.2 mm and 0.29 mm were considered SSW, and wear values greater than 0.3 mm were considered AW [15,22,61]. CNN models were trained using training and validation data and the tool wear stage was classified according to deep features. Finally, the trained networks were tested.

Table 5. Details of output and input of the CNN models for The NASA Ames Milling Dataset [21].

Input						Output
Vibration Spectrograms		Acoustic Emission Spectrograms		Motor Current Spectrograms		IW
Table	Spindle	Table	Spindle	AC	DC	SSW
Train, Validation, and Test Samples (50%, 30%, and %20)						AW
Cut of Depth		(0.75-1.5) mm				
Feed		(0.5-0.25) mm/rev				
Material		Steel and cast iron				

Table 6 indicates the output and input details of the CNN models for The 2010 PHM Data Challenge Dataset. Spectrograms of vibration signals, acoustic emission signals, and cutting force signals were obtained separately as 2D visual data. They are divided into three parts: training, validation, and test. CNN outputs have been modified to classify the tool wear stage. Accordingly, flank wear values in The 2010 PHM Data Challenge Dataset were evaluated as IW, SSW, and AW, similar to The Nasa Ames Milling Dataset. Similarly, CNN models

were trained using training, and validation data. The tool wear stage was classified according to the deep features, and finally, the trained networks were tested.

The 2010 PHM Data Challenge Dataset has records for six separate cutters (C1, C2, C3, C4, C5, and C6). However, tool wear data is available for only three of these records. Three records (C1, C4, and C6) of the aforementioned dataset were used in this study. 315 runs were performed separately for C1, C4, and C6 records.

Table 6 Details of output and input of the CNN models The 2010 PHM Data Challenge Dataset [1,54]

Input						Output	
Vibration Spectrograms			Cutting Force Spectrograms			Acoustic Emission Spectrograms	IW
x	y	z	x	y	z		SSW
Train, Validation, and Test Samples (50%, 30%, and %20)						AW	
Cut of Depth (y-direction)			0.125 mm				
Cut of Depth (z-direction)			0.2 mm				
Feed (x-direction)			1555 mm/min				

The difference in parameters such as feed rate and depth of cut given in Table 5 and Table 6 is due to the different test conditions in which two separate datasets were obtained [1, 21, 54]. In the test in Table 5, the feed rate of the device was set at different speeds, while in the test in Table 6, the feed rate of the device was configured at a constant speed.

3. Results and Discussion

3.1. Case 1: The NASA Ames Milling Dataset

3.1.1 Time-Frequency Signal Analysis for The NASA Ames Milling Dataset

This section includes the results from the signal processing and time-frequency analysis. In Fig. 7, the original signals from

The NASA Ames Milling Dataset and the spectrograms of these signals for a period of 0-1 s of case 1 can be seen.

The first dataset of case 1 consists of signals of vibration at the spindle (VS), vibration at the table (VT), acoustic emission at the spindle (AES), acoustic emission at the table (AET), AC spindle motor current (MAC) and DC spindle motor current (MDC). Looking at Fig. 7, it can be seen that the signals have three phases, namely the start phase, the operating phase, and the finishing phase. As can be shown from the spectrograms of the signals, the amplitudes and frequency spectrum values are low in the start phase. Signal amplitudes and frequency spectrum values increase during the operation phase and then decrease in the finishing phase.

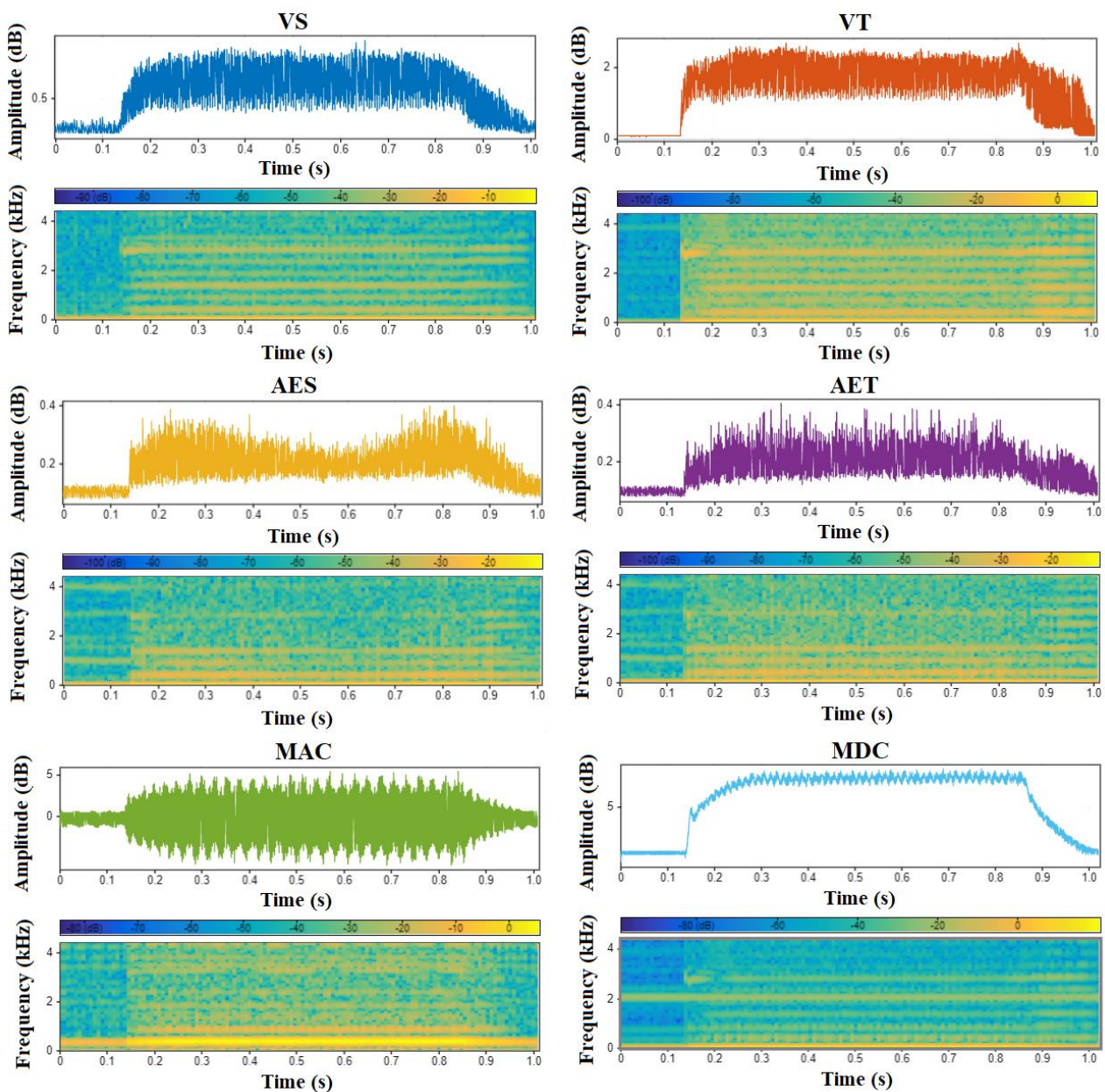


Fig. 7. Time and time-frequency domain representations of the different source signals.

3.1.2 Tool Wear Estimation Results with Different CNN Models for The NASA Ames Milling Dataset

In this study, milling tool wear estimation was performed using pre-trained CNN models. In the training of the models, spectrogram images obtained from vibration, acoustic emission, and motor current signal data were utilized. In the training

processes of CNNs, validation accuracies and loss values were calculated, weights of the networks were updated and the results of the models were also analyzed comparatively. Finally, the tool wear estimation models were tested with the reserved data and the performances of the models were compared with each other. In addition, CNN models were trained with different numbers of spectrograms and the results were analyzed.

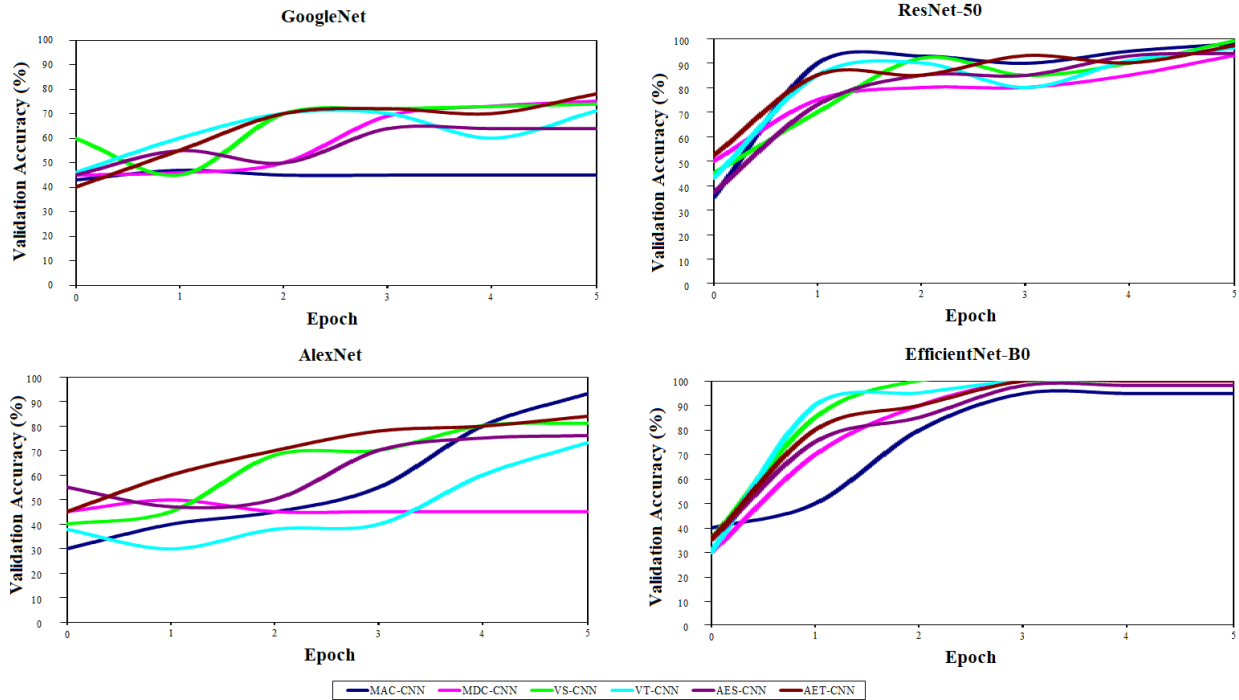


Fig. 8. Training accuracies of the CNN models.

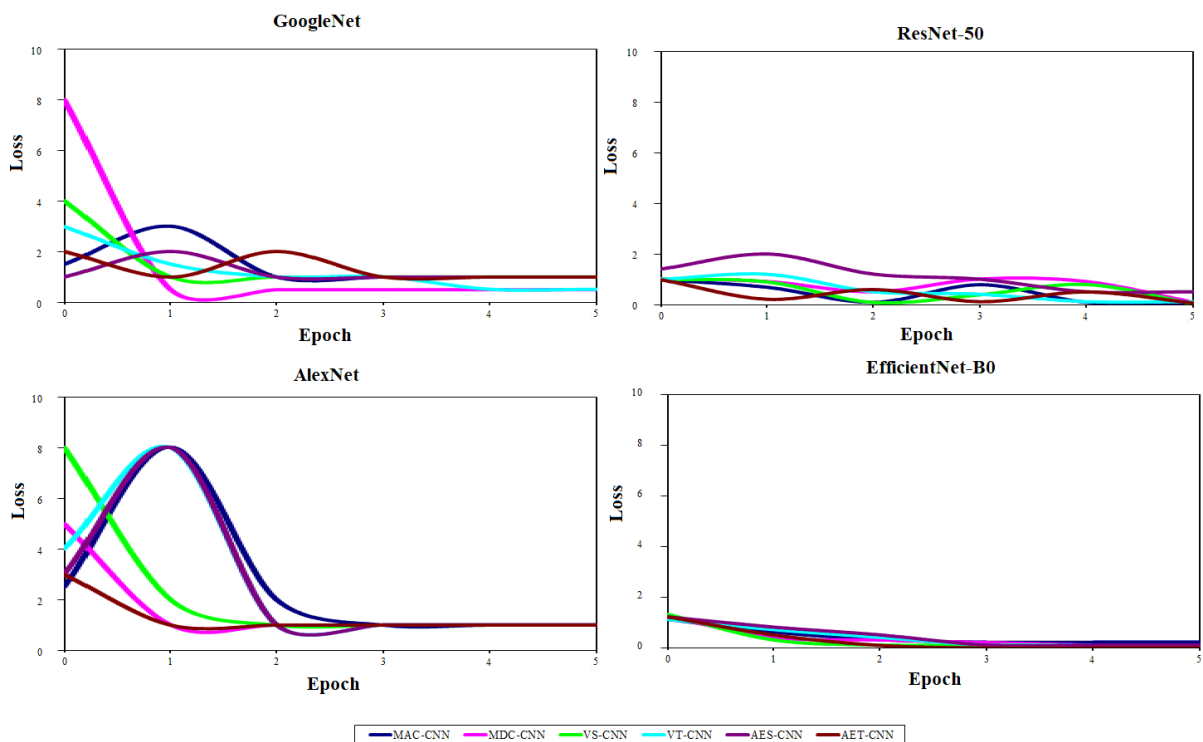


Fig. 9. The loss values of the CNN models.

Fig. 8 shows the variation in accuracies, and Fig. 9 shows the loss values during the training period for different CNN models. Accordingly, MAC-CNN is the model based on the AC signals of the spindle motor and MDC-CNN is the model based on the DC signals of the spindle motor. VS-CNN is the model based on vibration signals on the spindle, and VT-CNN is the model based on vibration signals on the table. Finally, AES-CNN is the model based on acoustic emission signals on the spindle, and AET-CNN is the model based on acoustic emission signals on the table. Table 7 shows the comparison of validation accuracies and test performances of models based on different pre-trained CNNs and trained with different numbers of spectrograms.

When Table 7, Fig. 8, and Fig 9 are examined together, it

can be understood that the validation accuracies of the models increase and the losses decrease as the epoch number increases. In addition, with the increase in the number of spectrograms, the model validation and test performances have increased. Looking at the GoogleNet-based CNN models, it can be seen that the highest validation and test performance rates are obtained with the AET-CNN models (Verification=0.80; Test=0.78). The lowest validation and test success were observed in the MAC-CNN model. When we look at the ResNet-based CNN models, it is seen that the validation and test performances of all models are above 90% for the case where the spectrogram is used the most. Results for CNN models based on EfficientNet-B0 are close to ResNet-50 but slightly higher. Performance values of AlexNet-based CNN models are lower than ResNet-50 and EfficientNet-B0 models.

Table 7. CNN models based on different numbers of spectrograms.

CNN Models	Spectrogram Number		Spectrogram Number		Spectrogram Number	
	IW=61; SSW=29; AW=75		IW=122; SSW=58; AW=150		IW=244; SSW=116; AW=300	
	Validation	Test	Validation	Test	Validation	Test
GoogleNet						
MAC-CNN	0.30	0.30	0.50	0.50	0.60	0.55
MDC-CNN	0.45	0.40	0.60	0.50	0.75	0.75
VS-CNN	0.37	0.35	0.65	0.60	0.74	0.70
VT-CNN	0.45	0.40	0.60	0.60	0.71	0.70
AES-CNN	0.37	0.30	0.55	0.50	0.64	0.60
AET-CNN	0.50	0.45	0.70	0.67	0.80	0.78
ResNet-50						
MAC-CNN	0.63	0.60	0.75	0.75	0.99	1
MDC-CNN	0.49	0.50	0.65	0.65	0.93	0.90
VS-CNN	0.59	0.55	0.70	0.70	0.99	1
VT-CNN	0.63	0.60	0.75	0.70	0.96	0.90
AES-CNN	0.69	0.65	0.70	0.65	0.94	0.90
AET-CNN	0.51	0.50	0.75	0.70	0.97	1
AlexNet						
MAC-CNN	0.45	0.45	0.65	0.65	0.93	0.90
MDC-CNN	0.37	0.40	0.50	0.50	0.70	0.70
VS-CNN	0.63	0.60	0.70	0.65	0.80	0.80
VT-CNN	0.57	0.55	0.65	0.60	0.73	0.70
AES-CNN	0.50	0.50	0.60	0.60	0.76	0.70
AET-CNN	0.39	0.35	0.65	0.60	0.84	0.80
EfficientNet-B0						
MAC-CNN	0.57	0.55	0.75	0.70	0.96	0.95
MDC-CNN	0.69	0.65	0.85	0.80	1	1
VS-CNN	0.61	0.60	0.87	0.85	1	0.98
VT-CNN	0.55	0.55	0.80	0.80	1	1
AES-CNN	0.67	0.65	0.85	0.85	0.98	0.95
AET-CNN	0.49	0.45	0.82	0.80	1	1

Fig. 10 shows the correlation between the number of spectrograms and the performance values of the models. Especially when high spectrogram numbers are used, the performance values of AET-CNN models come to the fore. In AlexNet-based CNNs, the performance values of MAC-CNN

models are higher. In general, there is no excessive difference between model performances. EfficientNet-B0-based MDC-CNN and VT-CNN models achieved 100% validation accuracy and classified the test data 100% correctly

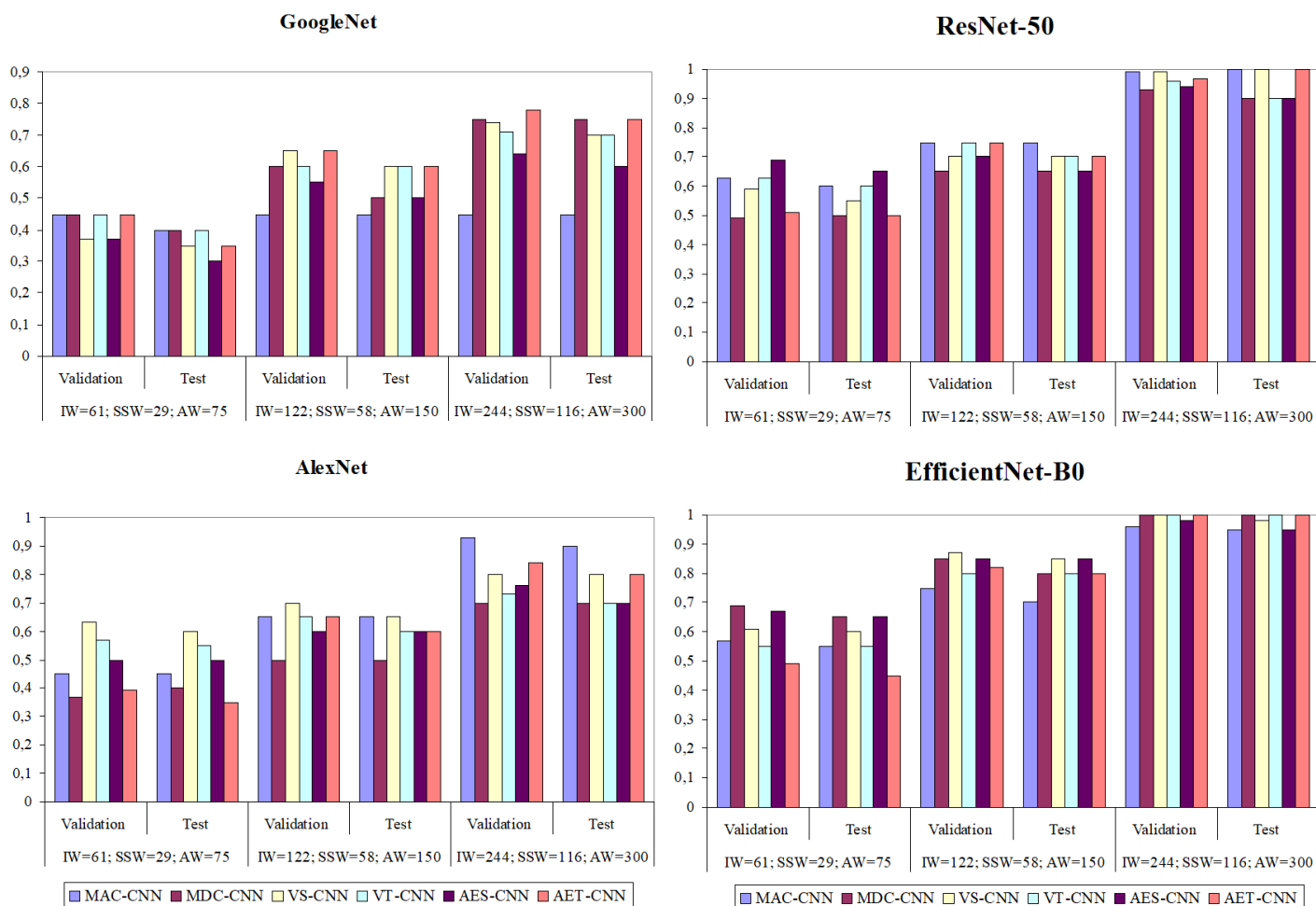


Fig. 10. The relationship between the number of spectrograms and the performance values of the models.

Table 8 shows the training periods of the CNN models trained with different numbers of spectrograms. Consequently, as the number of signal samples increases, the training times of all CNN models increase. It can be seen from the chart that CNNs with more complex architectures such as Resnet-50 and EfficientNet-B0 have a longer training period. The periods given in the table were obtained by running the MATLAB (2021-b) program on a computer with an Intel Core i7-3630QM, 2.40 GHz processor, and 16.0 GB of ram. It is obvious that training periods are reduced by using a more advanced computer or using different computers in parallel.

Each of the CNN models, whose validation and test results are given in Table 7, Fig. 8, Fig. 9, and Fig. 10, was developed

based on a single signal source. In this study, CNN models in which spectrograms of vibration signals, motor current signals, and acoustic emission signals are used together in the data set in order to determine the milling wear stage have also been developed. Table 9 indicates the validation and test performances of the CNN models acquired by using the spectrograms of all signals. In addition, Fig. 11 shows the training process and loss variation during the training of these models.

Table 8. The training periods of the CNN models.

CNN Models	Spectrogram Number	Spectrogram Number	Spectrogram Number
	IW=61; SSW=29; AW=75	IW=122; SSW=58; AW=150	IW=244; SSW=116; AW=300
	Training Time (s)	Training Time (s)	Training Time (s)
	GoogleNet		
MAC-CNN	171	425	1094
MDC-CNN	161	420	1051
VS-CNN	159	415	1056
VT-CNN	186	435	1053
AES-CNN	160	415	1061
AET-CNN	161	422	1181
ResNet-50			
MAC-CNN	446	1100	2922
MDC-CNN	433	1095	2740
VS-CNN	425	1080	2862
VT-CNN	419	1073	3183
AES-CNN	432	1090	2894
AET-CNN	434	1097	2857
AlexNet			
MAC-CNN	80	356	1089
MDC-CNN	88	365	1035
VS-CNN	87	360	1206
VT-CNN	87	359	1021
AES-CNN	86	343	1147
AET-CNN	89	345	1080
EfficientNet-B0			
MAC-CNN	337	1522	4142
MDC-CNN	343	1634	3937
VS-CNN	360	1765	4122
VT-CNN	374	1892	4214
AES-CNN	376	1903	4276
AET-CNN	388	1986	3987

Table 9. shows the validation and test performances of the CNN models.

CNN	Total Spectrogram Numbers (Included All Signal Sources)		
	IW=366; SSW=174; AW=450		
	Validation	Test	Training Time (s)
GoogleNet-CNN	0.51	0.50	2221
ResNet-50-CNN	0.67	0.65	5206
AlexNet-CNN	0.37	0.30	1050
EfficientNet-B0-CNN	0.63	0.60	3773

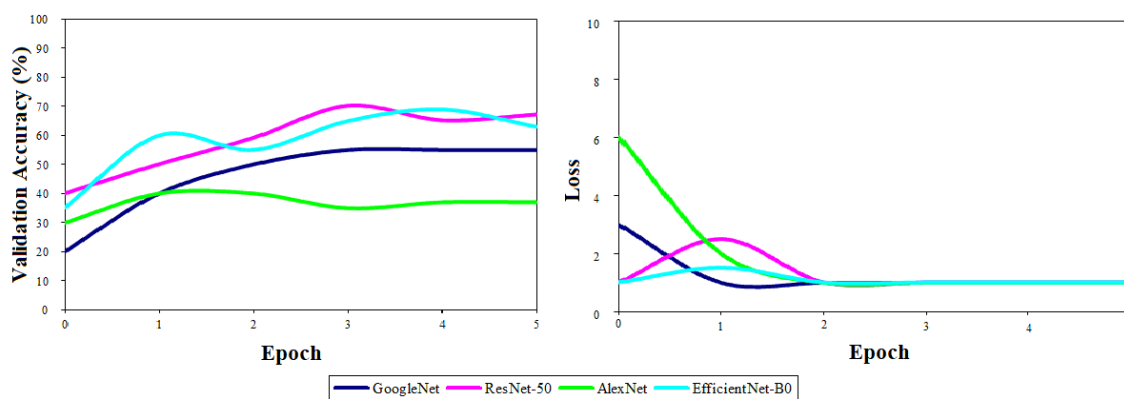


Fig. 11. The training process and loss variation of CNN models based on multiple signal sources.

When Table 9 and Fig. 11 are investigated together, it can be seen that CNN models with more complex architecture have higher validation accuracy and test success. Additively, the training times of these models are longer than the CNN models with simpler architecture. Considering the results obtained from CNN models using a single signal source, the use of spectrograms obtained from different signal sources together in the same data set adversely affected the model performance.

3.2. Case 2: The 2010 PHM Data Challenge Dataset

3.2.1 Time-Frequency Signal Analysis for The 2010 PHM Data Challenge Dataset

This section includes the results from the signal processing

and time-frequency analysis for The 2010 PHM Data Challenge Dataset. In Fig. 12, the original signals from the dataset and the spectrograms of these signals in the 0-2.5 s time interval are shown. The first dataset of C1 consists of signals of vibration (V_x , V_y , and V_z), cutting force (F_x , F_y , and F_z), and acoustic emission (AE).

Looking at Fig. 12, it can be seen that the vibration signals in the x, z, and y directions are very similar. However, when the measurements of the shear force in three directions are examined, it is understood that they differ slightly from each other. Also, time and time-frequency domain representations of acoustic emission signals can be seen in Fig. 12.

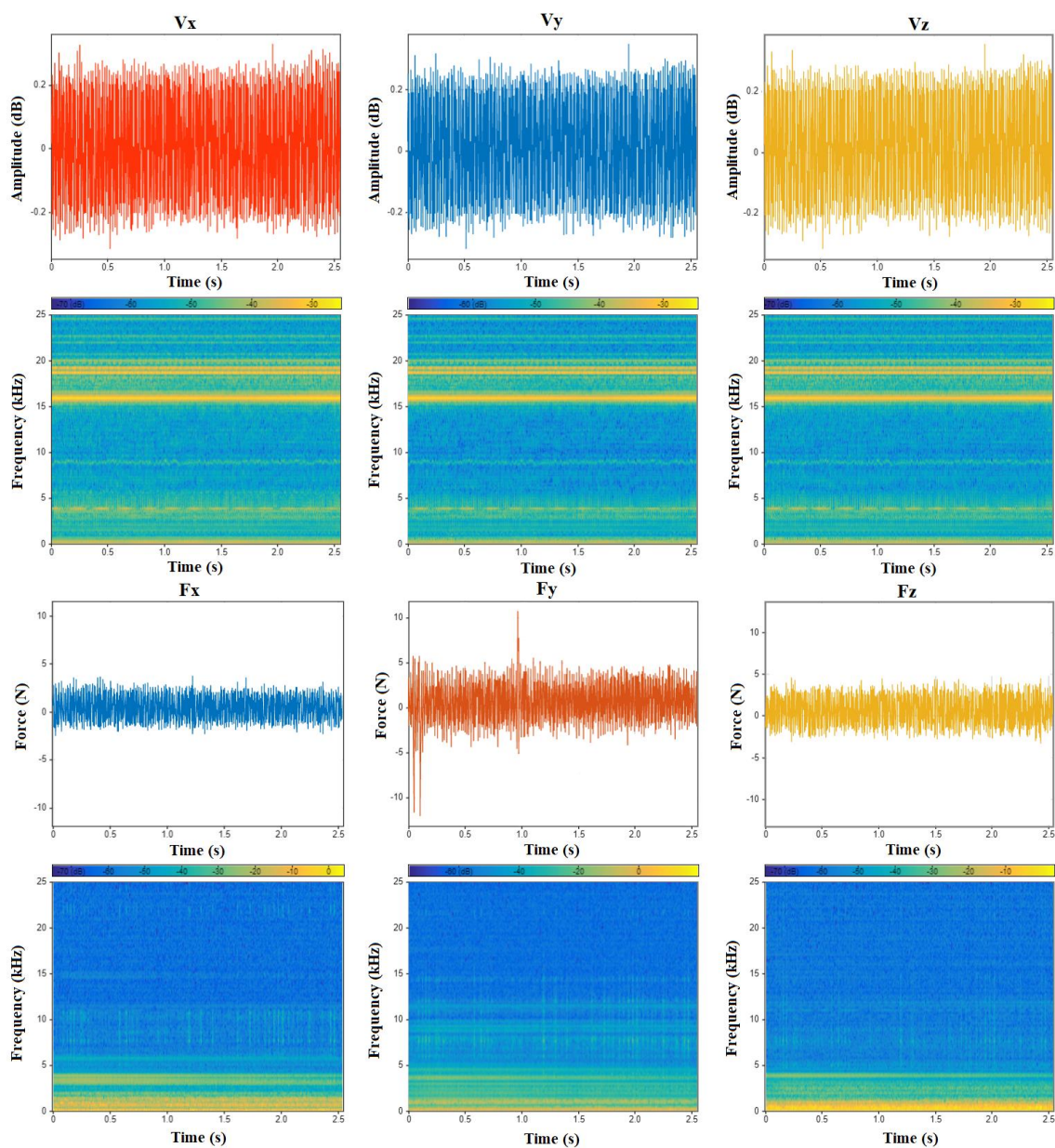


Fig. 12. Time and time-frequency domain representations of the cutting force and vibration signals.

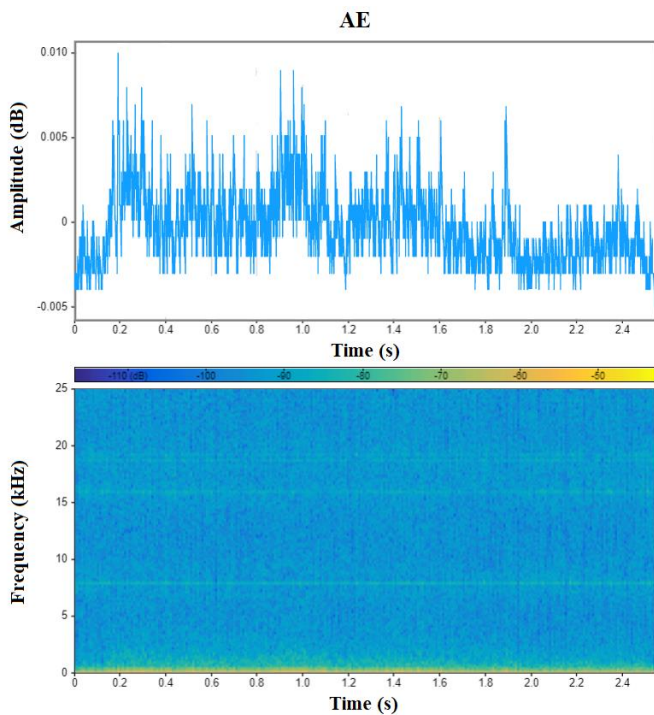


Fig. 13. Time and time-frequency domain representations of the acoustic emission signals.

3.2.2 Tool Wear Estimation Results with Different CNN Models for The 2010 PHM Data Challenge Dataset

In this section, milling tool wear was estimated using pre-trained CNN models using The 2010 PHM Data Challenge Dataset. In the training of the models, spectrogram images obtained from vibration, acoustic emission, and shear force data were used. In the training periods of CNNs, validation accuracies and loss values were calculated, the weights of the

networks were updated and the results of the models were analyzed comparatively. Finally, the tool wear prediction models were tested with the separated data, and the performances of the models were compared with each other.

Table 10 shows the accuracies and test performances for different CNN models. Accordingly, Vxyz-CNN is the model based on vibration signals, Fxyz-CNN is the model based on cutting force signals, and AE-CNN is the model based on acoustic emission signals. In order not to cause an abundance of graphics and tables, we have not included tables and figures regarding the training details of the models here.

When Table 10 is examined, it can be seen that the validation accuracies of the models increase as the number of spectrograms increases. Looking at the GoogleNet-based CNN models, it can be seen that the highest validation and test performance rates are obtained with the Vxyz-CNN models. The lowest validation and test successes were observed in the AE-CNN models. When we look at the ResNet and EfficientNet-B0 based CNN models, it is seen that the validation and test performances of all models are 100% for the cases where the spectrogram is used the most. Performance values of AlexNet-based CNN models are lower than GoogleNet, ResNet-50, and EfficientNet-B0 models. The table also shows the relationship between the number of spectrograms and the performance values of the models. Especially when high spectrogram numbers are used, the performance values of some models are 100%.

Table 10. CNN models based on different numbers of spectrograms.

CNN Models	Spectrogram Number		Spectrogram Number		Spectrogram Number	
	IW=12; SSW=36; AW=24		IW=24; SSW=72; AW=48		IW=48; SSW=144; AW=96	
	Validation	Test	Validation	Test	Validation	Test
	GoogleNet					
Vxyz-CNN	0.90	0.80	0.95	0.90	1	1
Fxyz-CNN	0.82	0.70	0.84	0.80	1	0.95
AE-CNN	0.80	0.70	0.80	0.80	1	0.95
	ResNet-50					
Vxyz-CNN	0.95	0.90	1	0.95	1	1
Fxyz-CNN	0.95	0.95	1	0.95	1	1
AE-CNN	0.95	0.95	1	0.95	1	1
	AlexNet					
Vxyz-CNN	0.40	0.30	0.45	0.30	0.50	0.40
Fxyz-CNN	0.50	0.40	0.67	0.50	0.80	0.70
AE-CNN	0.50	0.40	0.75	0.65	0.90	0.80
	EfficientNet-B0					

CNN Models	Spectrogram Number		Spectrogram Number		Spectrogram Number	
	IW=12; SSW=36; AW=24		IW=24; SSW=72; AW=48		IW=48; SSW=144; AW=96	
	Validation	Test	Validation	Test	Validation	Test
	GoogleNet					
Vxyz-CNN	1	0.95	1	1	1	1
Fxyz-CNN	1	1	1	1	1	1
AE-CNN	1	0.90	1	0.95	1	1

Table 11. The training periods of the CNN models.

CNN Models	Spectrogram Number		Spectrogram Number		Spectrogram Number	
	IW=12; SSW=36; AW=24		IW=24; SSW=72; AW=48		IW=48; SSW=144; AW=96	
	Training Time (s)		Training Time (s)		Training Time (s)	
	GoogleNet					
Vxyz-CNN	61		135		345	
Fxyz-CNN	62		137		351	
AE-CNN	62		147		372	
	ResNet-50					
Vxyz-CNN	152		334		806	
Fxyz-CNN	147		326		785	
AE-CNN	147		320		750	
	AlexNet					
Vxyz-CNN	35		70		140	
Fxyz-CNN	35		74		161	
AE-CNN	35		74		164	
	EfficientNet-B0					
Vxyz-CNN	133		333		810	
Fxyz-CNN	130		325		790	
AE-CNN	130		328		795	

In this study, spectrograms used in deep learning models for both Case 1 and Case 2 were obtained by applying short-time Fourier transform (STFT) to all signals. No cutoff frequency was applied during the acquisition of the spectrograms. The absence of a cutoff frequency did not impact our ability to analyze the frequency content of the signals and detect the stage of tool wear. However, if the performances of the models were low, applying a cutoff frequency may be necessary. Additionally, if different signal ranges are to be examined in detail for further analysis, a cutoff should be applied.

Vibration, acoustic, AC, and DC signals from the spindle motor were captured using specialized sensors. However, frequency calculations based on spindle speed were not

performed in our study. Rather, we obtained spectrograms of the vibration, acoustic, and motor current signals and used them to detect tool wear stage. By analyzing the frequency content of the signals over time, we were able to identify changes in spectral characteristics that corresponded to changes in cutting conditions and tool wear. While frequency calculations based on spindle speed could have provided additional information, our approach of using spectrograms allowed us to capture more comprehensive information about the tool wear process and enabled us to develop a robust tool wear stage detection method that can be applied to various machining conditions.

In our study, we did not perform frequency calculations from the radial runout of individual cutter blades. However, we

acknowledge that radial runout has a significant impact on the wear of individual tool blades. Our study focused on analyzing the signals from the sensors and using spectrograms to detect tool wear stage. Future works can explore the relationship between the radial runout of the cutting blades and the corresponding frequency content of the signals, which can provide useful information regarding the tool wear process.

4. Conclusions

In this study, a method based on deep learning and different source signals, which takes into account the wear stages holistically, is proposed for the timely and accurate detection of tool wear. Milling tool wear stage estimation was performed using the CNN models based on signal 2D spectrograms obtained from The Nasa Ames Milling Dataset and The 2010 PHM Data Challenge Dataset. CNN models with different architectures were trained and tested with spectrograms for tool wear stage estimation, and the results were examined comparatively. According to the results of the study, the conclusions can be expressed as follows.

- The tool wear stage can be estimated by utilizing a single signal source with CNN models with more complex architecture.
- The simultaneous use of multiple signal sources reduces the success of the models.
- With a sufficient number of spectrograms, all CNN models based on Resnet-50 and EfficientNet-B0 achieved over 90% validation accuracy and test success for both datasets.
- For The Nasa Ames Milling Dataset, the models based on acoustic emission and AC motor current signals gave more successful results.
- For the 2010 PHM Data Challenge Dataset, the models based on vibration signals are more successful.
- The reason of differences of results for both datasets can be explained as the differences in the details of the measurements of the signals, the differences in the experimental systems, and the differences in working conditions.
- As the CNN architecture gets more complex, the number of layers gets deeper and the number of spectrograms used increases, it has been seen that the training duration gets longer. Because 2D spectrograms are processed in each layer and the outputs obtained are used as inputs for the next layer.
- The negative effect of the layer depth on the diagnostic time should be taken into consideration when determining the milling tool wear stage.

References

1. 2010 PHM Data Challenge. https://phmsociety.org/phm_competition/2010-phm-society-conference-data-challenge/
2. Aghazadeh F, Tahan A, Thomas M. Tool condition monitoring using spectral subtraction and convolutional neural networks in milling process. *The International Journal of Advanced Manufacturing Technology* 2018;98(9):3217-3227. <https://doi.org/10.1007/s00170-018-2420-0>
3. Aliustaoglu C, Ertunc HM, Ocak H. Tool wear condition monitoring using a sensor fusion model based on fuzzy inference system. *Mechanical Systems and Signal Processing* 2009;23(2):539-546. <https://doi.org/10.1016/j.ymssp.2008.02.010>
4. Alzubaidi L, Zhang J, Humaidi AJ, Al-Dujaili A, Duan Y, Al-Shamma O, Farhan L. Review of deep learning: Concepts, CNN architectures, challenges, applications, future directions. *Journal of Big Data* 2021;8(1):1-74. <https://doi.org/10.1186/s40537-021-00444-8>
5. Ambadekar PK, Choudhari CM. CNN based tool monitoring system to predict life of cutting tool. *SN Applied Sciences* 2020;2(5):1-11. <https://doi.org/10.1007/s42452-020-2598-2>
6. Arinez JF, Chang Q, Gao RX, Xu C, Zhang J. Artificial intelligence in advanced manufacturing: Current status and future Outlook. *Journal of Manufacturing Science and Engineering* 2020;142(11):110804. <https://doi.org/10.1115/1.4047855>
7. Bagga PJ, Makhesana MA, Patel HD, Patel KM. Indirect method of tool wear measurement and prediction using ANN network in machining process. *Material Today: Proceedings* 2021;44:1549-1554. <https://doi.org/10.1016/j.matpr.2020.11.770>
8. Bazi R, Benkedjough T, Habbouche H, Rechak S, Zerhouni N. A hybrid CNN-BiLSTM approach-based variational mode decomposition for tool wear monitoring. *The International Journal of Advanced Manufacturing Technology* 2022;119(5):3803-3817. <https://doi.org/10.1007/s00170-021-08448-7>
9. Bergs T, Holst C, Gupta P, Augspurger T. Digital image processing with deep learning for automated cutting tool wear detection. *Procedia*

- Manufacturing 2020;48:947-958. <https://doi.org/10.1016/j.promfg.2020.05.134>
10. Brili N, Ficko M, Klancnik S. Automatic identification of tool wear based on thermography and a convolutional neural network during the turning process. *Sensors* 2021;21(5):1917. <https://doi.org/10.3390/s21051917>
 11. Cao X, Chen B, Yao B, Zhuang S. An intelligent milling tool wear monitoring methodology based on convolutional neural network with derived wavelet frames coefficient. *Applied Sciences* 2019;9(18):3912. <https://doi.org/10.3390/app9183912>
 12. Cao XC, Chen BQ, Yao B, He WP. Combining translation-invariant wavelet frames and convolutional neural network for intelligent tool wear state identification. *Computers in Industry* 2019;106:71-84. <https://doi.org/10.1016/j.compind.2018.12.018>
 13. Chen JC, Susanto V. Fuzzy logic based in-process tool-wear monitoring system in face milling operations. *The International Journal of Advanced Manufacturing Technology* 2003;21(3):186-192. <https://doi.org/10.1007/s001700300020>
 14. Chen XQ, Li HZ. Development of a tool wear observer model for online tool condition monitoring and control in machining nickel-based alloys. *The International Journal of Advanced Manufacturing Technology* 2009;45(7):786-800. <https://doi.org/10.1007/s00170-009-2003-1>
 15. Chung TK, Yeh PC, Lee H, Lin CM, Tseng CY, Lo WT, Chang JW. An Attachable Electromagnetic Energy Harvester Driven Wireless Sensing System Demonstrating Milling Processes and Cutter Wear Breakage Condition monitoring. *Sensors* 2016;16(3):269. <https://doi.org/10.3390/s16030269>
 16. Colantonio L, Equeter L, Dehombreux P, Ducobu F. A systematic literature review of cutting tool wear monitoring in turning by using artificial intelligence techniques. *Machines* 2021;9(12):351. <https://doi.org/10.3390/machines9120351>
 17. Cooper C, Wang P, Zhang J, Gao RX, Roney T, Ragai I, Shaffer D. Convolutional neural network-based tool condition monitoring in vertical milling operations using acoustic signals. *Procedia Manufacturing* 2020;49:105-111. <https://doi.org/10.1016/j.promfg.2020.07.004>
 18. Dai W, Liang K, Wang B. State Monitoring Method for Tool Wear in Aerospace Manufacturing Processes Based on a Convolutional Neural Network (CNN). *Aerospace* 2021;8(11):335. <https://doi.org/10.3390/aerospace8110335>
 19. Duan J, Duan J, Zhou H, Zhan X, Li T, Shi T. Multi-frequency-band deep CNN model for tool wear prediction. *Measurement Science and Technology* 2021;32(6):065009. <https://doi.org/10.1088/1361-6501/abb7a0>
 20. Emmert-Streib F, Yang Z, Feng H, Tripathi S, Dehmer M. An introductory review of deep learning for prediction models with big data. *Frontiers in Artificial Intelligence* 2020;3:4. <https://doi.org/10.3389/frai.2020.00004>
 21. Goebel K. Management of Uncertainty in Sensor Validation, Sensor Fusion, and Diagnosis of Mechanical Systems Using Soft Computing Techniques. PhD Thesis, Department of Mechanical Engineering, University of California at Berkeley:1996.
 22. Groover MP. *Fundamentals of Modern Manufacturing: Materials, Processes, and Systems*. NJ, John Wiley & Sons, Inc:2010
 23. Gu J, Wang Z, Kuen J, Ma L, Shahroudy A, Shuai B, Chen T. Recent advances in convolutional neural Networks. *Pattern Recognition* 2018;77:354-377. <https://doi.org/10.1016/j.patcog.2017.10.013>
 24. Habrat W, Krupa K, Markopoulos AP, Karkalos NE. Thermo-mechanical aspects of cutting forces and tool wear in the laser-assisted turning of Ti-6Al-4V titanium alloy using AlTiN coated cutting tools. *The International Journal of Advanced Manufacturing Technology* 2021;115(3):759-775. <https://doi.org/10.1007/s00170-020-06132-w>
 25. Hao X, Zheng Y, Lu L, Pan H. Research on Intelligent Fault Diagnosis of Rolling Bearing Based on Improved Deep Residual Network. *Applied Sciences* 2021;11(22):10889. <https://doi.org/10.3390/app112210889>
 26. Huang PM, Lee CH. Estimation of tool wear and surface roughness development using deep learning and sensors fusion. *Sensors* 2021;21(16) 5338. <https://doi.org/10.3390/s21165338>
 27. Huang Z, Zhu J, Lei J, Li X, Tian F. Tool wear monitoring with vibration signals based on short-time fourier transform and deep convolutional neural network in milling. *Mathematical Problems in Engineering* 2021;9976939. <https://doi.org/10.1155/2021/9976939>
 28. Huang Z, Zhu J, Lei J, Li X, Tian F. Tool wear predicting based on multi-domain feature fusion by deep convolutional neural network in milling operations. *Journal of Intelligent Manufacturing* 2020;31(4):953-966. <https://doi.org/10.1007/s10845-019-01488-7>
 29. Huang Z, Zhu J, Lei J, Li X, Tian F. Tool wear predicting based on multisensory raw signals fusion by reshaped time series convolutional neural network in manufacturing, *IEEE Access* 2019;7:178640-178651. <https://doi.org/10.1109/ACCESS.2019.2958330>
 30. Jeon H, Jung Y, Lee S, Jung Y. Area-Efficient Short-Time Fourier Transform Processor for Time–Frequency Analysis of Non-Stationary Signals. *Applied Sciences* 2020;10(20):7208. <https://doi.org/10.3390/app10207208>

31. Jing L, Zhao M, Li P, Xu X. A convolutional neural network based feature learning and fault diagnosis method for the condition monitoring of gearbox. *Measurement* 2017;111:1-10. <https://doi.org/10.1016/j.measurement.2017.07.017>
32. Karabacak YE, Gürsel Özmen N, Gümüsel L. Worm gear condition monitoring and fault detection from thermal images via deep learning method. *Eksplatacja i Niezawodność – Maintenance and Reliability* 2020;22(3):544–556. <http://dx.doi.org/10.17531/ein.2020.3.18>
33. Kilundu B, Dehombreux P, Chimentin X. Tool wear monitoring by machine learning techniques and singular spectrum analysis. *Mechanical Systems and Signal Processing* 2011;25(1):400-415. <https://doi.org/10.1016/j.ymssp.2010.07.014>
34. Kong D, Chen Y, Li N. Gaussian process regression for tool wear prediction. *Mechanical Systems and Signal Processing* 2018;104:556-574. <https://doi.org/10.1016/j.ymssp.2017.11.021>
35. Li G, Wang Y, Wang J, He J, Huo Y. Tool wear prediction based on multidomain feature fusion by attention-based depth-wise separable convolutional neural network in manufacturing. *The International Journal of Advanced Manufacturing Technology* 2021;1-18. <https://doi.org/10.1007/s00170-021-08119-7>
36. Li W, Liu T. Time varying and condition adaptive hidden Markov model for tool wear state estimation and remaining useful life prediction in micro-milling. *Mechanical Systems and Signal Processing* 2019;131:689-702. <https://doi.org/10.1016/j.ymssp.2019.06.021>
37. Liao X, Zhou G, Zhang Z, Lu J, Ma J. Tool wear state recognition based on GWO–SVM with feature selection of genetic algorithm. *The International Journal of Advanced Manufacturing Technology* 2019;104(1):1051-1063. <https://doi.org/10.1007/s00170-019-03906-9>
38. Lim ML, Derani MN, Ratnam MM, Yusoff AR. Tool wear prediction in turning using workpiece surface profile images and deep learning neural Networks. *The International Journal of Advanced Manufacturing Technology* 2022;120(11):8045-8062. <https://doi.org/10.1007/s00170-022-09257-2>
39. Liu H, Liu Z, Jia W, Zhang D, Wang Q, Tan J. Tool wear estimation using a CNN-transformer model with semi-supervised learning. *Measurement Science and Technology* 2021;32(12):125010. <https://doi.org/10.1088/1361-6501/ac22ee>
40. Ma J, Luo D, Liao X, Zhang Z, Huang Y, Lu J. Tool wear mechanism and prediction in milling TC18 titanium alloy using deep learning. *Measurement* 2021;173:108554. <https://doi.org/10.1016/j.measurement.2020.108554>
41. Mohanraj T, Shankar S, Rajasekar R, Sakthivel NR, Pramanik A. Tool condition monitoring techniques in milling process—a review. *Journal of Materials Research and Technology* 2020;9(1):1032-1042. <https://doi.org/10.1016/j.jmrt.2019.10.031>
42. Nouioua M, Bouhalais ML. Vibration-based tool wear monitoring using artificial neural networks fed by spectral centroid indicator and RMS of CEEMDAN modes. *The International Journal of Advanced Manufacturing Technology* 2021;115(9):3149-3161. <https://doi.org/10.1007/s00170-021-07376-w>
43. Olsson M, Bushlya V, Lenrick F, Stahl JE. Evaluation of tool wear mechanisms and tool performance in machining single-phase tungsten. *International Journal of Refractory Metals and Hard Materials* 2021;94:105379. <https://doi.org/10.1016/j.ijrmhm.2020.105379>
44. Patange AD, Jegadeeshwaran R. Review on tool condition classification in milling: A machine learning approach. *Material Today: Proceedings* 2021;46:1106-1115. <https://doi.org/10.1016/j.matpr.2021.01.523>
45. Pimenov DY, Gupta MK, da Silva LR, Kiran M, Khanna N, Krolczyk GM. Application of measurement systems in tool condition monitoring of Milling: A review of measurement science approach. *Measurement* 2022;199:111503. <https://doi.org/10.1016/j.measurement.2022.111503>
46. Pimenov DY, Mia M, Gupta MK, Machado AR, Pintaude G, Unune DR, Kuntoğlu M. Resource saving by optimization and machining environments for sustainable manufacturing: A review and future prospects. *Renewable and Sustainable Energy Reviews* 2022;166:112660. <https://doi.org/10.1016/j.rser.2022.112660>
47. Saha S, Deb S, Bandyopadhyay PP. Progressive wear based tool failure analysis during dry and MQL assisted sustainable micro-milling. *International Journal of Mechanical Sciences* 2021;212:106844. <https://doi.org/10.1016/j.ijmecsci.2021.106844>
48. Serin G, Sener B, Ozbayoglu AM, Unver HO. Review of tool condition monitoring in machining and opportunities for deep learning. *The International Journal of Advanced Manufacturing Technology* 2020;109(3):953-974. <https://doi.org/10.1007/s00170-020-05449-w>
49. Serra R, Rmili W. Experimental evaluation of flank wear in dry turning from accelerometer data. *International Journal of Acoustics and Vibration* 2016;21(1):50-58. <http://dx.doi.org/10.20855/ijav.2016.21.1394>
50. Shao F, Liu Z, Wan Y. Diffusion and oxidation wear of PCBN tool based on thermodynamics. *Journal of Wuhan University of Technology-Mater. Sci. Ed.* 2010;25(2):265-271. <https://doi.org/10.1007/s11595-010-2265-3>

51. Terrazas G, Martinez-Arellano G, Benardos P, Ratchev S. Online tool wear classification during dry machining using real time cutting force measurements and a CNN approach. *Journal of Manufacturing and Materials Processing* 2018;2(4):72. <https://doi.org/10.3390/jmmp2040072>
52. Trejo-Hernandez M, Osornio-Rios RA, de Jesus Romero-Troncoso R, Rodriguez-Donate C, Dominguez-Gonzalez A, Herrera-Ruiz G. FPGA-based fused smart-sensor for tool-wear area quantitative estimation in CNC machine inserts. *Sensors* 2010;10(4):3373-3388. <https://doi.org/10.3390/s100403373>
53. Vetrichelvan G, Sundaram S, Kumaran SS, Velmurugan P. An investigation of tool wear using acoustic emission and genetic algorithm. *Journal of Vibration and Control* 2015;21(15):3061-3066. <https://doi.org/10.1177/1077546314520835>
54. Wang J, Xie J, Zhao R, Zhang L, Duan L. Multisensory fusion based virtual tool wear sensing for ubiquitous manufacturing. *Robotics and Computer-Integrated Manufacturing* 2017;45:47-58. <https://doi.org/10.1016/j.rcim.2016.05.010>
55. Wang Q, Wang H, Hou L, Yi S. Overview of Tool Wear Monitoring Methods Based on Convolutional Neural Network. *Applied Sciences* 2021;11(24):12041. <https://doi.org/10.3390/app112412041>
56. Wu J, Su Y, Cheng Y, Shao X, Deng C, Liu C. Multi-sensor information fusion for remaining useful life prediction of machining tools by adaptive network based fuzzy inference system. *Applied Soft Computing* 2018; 68:13-23. <https://doi.org/10.1016/j.asoc.2018.03.043>
57. Wu X, Liu Y, Zhou X, Mou A. Automatic identification of tool wear based on convolutional neural network in face milling process. *Sensors* 2019;19(18):3817. <https://doi.org/10.3390/s19183817>
58. Xu X, Wang J, Zhong B, Ming W, Chen M. Deep learning-based tool wear prediction and its application for machining process using multi-scale feature fusion and channel attention mechanism. *Measurement* 2021;177:109254. <https://doi.org/10.1016/j.measurement.2021.109254>
59. Yamashita R, Nishio M, Do RKG, Togashi K. Convolutional neural networks: an overview and application in radiology. *Insights into Imaging* 2018;9(4):611-629. <https://doi.org/10.1007/s13244-018-0639-9>
60. Yin Y, Wang S, Zhou J. Multisensor-based tool wear diagnosis using 1D-CNN and DGCCA. *Applied Intelligence* 2022;1-14. <https://doi.org/10.1007/s10489-022-03773-0>
61. Younas M, Jaffery SHI, Khan A, Khan M. Development and analysis of tool wear and energy consumption maps for turning of titanium alloy (Ti6Al4V). *Journal of Manufacturing Processes* 2021;62:613-622. <https://doi.org/10.1016/j.jmapro.2020.12.060>
62. Zhang X, Lu X, Li W, Wang S. Prediction of the remaining useful life of cutting tool using the Hurst exponent and CNN-LSTM. *The International Journal of Advanced Manufacturing Technology* 2021;112(7):2277-2299. <https://doi.org/10.1007/s00170-020-06447-8>
63. Zheng G, Sun W, Zhang H, Zhou Y, Gao C. Tool wear condition monitoring in milling process based on data fusion enhanced long short-term memory network under different cutting conditions. *Eksplotacja i Niezawodność-Maintenance and Reliability* 2021;23(4):612-618. <https://doi.org/10.17531/ein.2021.4.3>
64. Zhou Y, Zhi G, Chen W, Qian Q, He D, Sun B, Sun W. A new tool wear condition monitoring method based on deep learning under small samples. *Measurement* 2022;189:110622. <https://doi.org/10.1016/j.measurement.2021.110622>
65. Zhu Q, Sun W, Zhou Y, Gao C. A tool wear condition monitoring approach for end milling based on numerical simulation. *Eksplotacja i Niezawodność-Maintenance and Reliability* 2021;23(2):371-380. <https://doi.org/10.17531/ein.2021.2.17>